ACADEMIC PRESS

Available online at www.sciencedirect.com
SCIENCE DIRECT®

Journal of Catalysis 213 (2003) 176–190

JOURNAL OF CATALYSIS

www.elsevier.com/locate/jcat

The kinetics of methanol oxidation on a supported Pd model catalyst: molecular beam and TR-IRAS experiments

J. Hoffmann, S. Schauermann, V. Johánek, J. Hartmann, and J. Libuda *

Fritz-Haber-Institut der Max-Planck-Gesellschaft, Faradayweg 4-6, 14195 Berlin, Germany

Received 24 May 2002; revised 16 August 2002; accepted 1 September 2002

Abstract

Combining a multi-molecular-beam approach and in situ time-resolved IR reflection absorption spectroscopy (TR-IRAS), we investigate the kinetics of methanol oxidation on a well-defined supported Pd model catalyst. The model catalyst is prepared under ultra-high-vacuum (UHV) conditions by Pd deposition onto a well-ordered Al_2O_3 film grown on NiAl (110). In previous studies, this system has been characterized in detail with respect to its geometric and electronic structure and its adsorption properties. Crossing molecular beams of methanol and oxygen on the sample surface, we systematically probe the rate of total methanol oxidation to CO_2 as a function of surface temperature and reactant fluxes. The results are compared with equivalent experiments for the related CO oxidation reaction. Pronounced differences are observed in the kinetics of the two processes, both under steady state and under transient conditions. The dissimilarities can be related to the dehydrogenation step of methanol, which is found to be strongly inhibited at high oxygen coverage. At low oxygen fluxes, CO is formed as the main product of methanol decomposition. Via a three-beam isotope-exchange experiment combined with TR-IRAS, the kinetics of CO formation is investigated as a function of reactant fluxes and surface temperature. Mean-field simulations of the kinetics are performed in a two-step procedure. First, the kinetics of CO oxidation is described, both under steady state and transient conditions. In a second step the microkinetic model is extended to include the formation of CO formed by methanol dehydrogenation. A comparison with the experimental data indicates that the transient kinetics cannot be fully described by a mean-field approach.

Keywords: Supported model catalysts; Methanol; Palladium; Alumina; Molecular beams; IR reflection absorption spectroscopy; Microkinetic simulations

1. Introduction

In many cases, the kinetics of heterogeneously catalyzed reactions sensitively depend on the particle size and structure, the support material, or the presence of promotors and poisons. In the literature, the possible role of such effects has been discussed for a long time (see, e.g., [1]). On a molecular basis, however, little is known of reaction kinetics on the complex surfaces of supported catalysts (see, e.g., [2,3]).

The lack of thorough understanding is essentially the result of two problems: (1) Precise *structural and chemical characterization* proves to be extremely difficult for the surfaces of most real catalysts. Single crystals, on the other hand, which are well defined on an atomic basis, do not show the effects under consideration. (2) If available, the structural characteristics of the catalytically active surface have to be correlated with *detailed experimental data on the surface kinetics*. This type of precise and quantitative kinetic data, however, are scarce for simple surfaces and are missing almost completely for well-defined but complex surfaces.

In order to surmount these difficulties, we follow a model catalyst approach. Supported model catalysts allow us to design surfaces that resemble specific features of real catalysts [2–6]. Still, these systems provide a reduced level of complexity and can be easily probed using a variety of surface science techniques. In this work, we use a Pd model catalyst, which is prepared under UHV (ultra-high-vacuum) conditions, based on an ordered alumina film grown on a NiAl (110) single crystal [7,8]. Both, the geometric and electronic structure of the system, as well as its adsorption properties, have been investigated previously (see, e.g., [4, 9–11] and references therein).

In order to perform detailed and quantitative kinetic measurements on these well-defined model catalysts, we employ molecular beam techniques. Molecular beam methods have been successfully applied to several reaction systems on sin-

* Corresponding author.
E-mail address: libuda@fhi-berlin.mpgde (J. Libuda).

0021-9517/02/$ – see front matter
PII: S0021-9517(02)00029-5

gle crystals (see, e.g., [12–14] and references therein). On supported model catalysts, however, the amount of work is limited and the few studies performed so far focus entirely on simple reaction systems such as CO oxidation (see, e.g., [3,15,16] and references therein) or the NO–CO reaction (see, e.g., [17,18]).

In our experiments we combine multiple beam sources with simultaneous gas phase detection and in situ time-resolved IR reflection absorption spectroscopy (TR-IRAS [19]). Recently, we applied this approach to the CO oxidation on different types of supported Pd model catalysts [20,21]. On the basis of these experiments, it was possible to derive a microkinetic model, which provides a good description of the kinetics, both under steady state and transient conditions [22].

In this study, we attempt to extend this type of work toward more complex reaction systems, focusing on the decomposition and total oxidation of methanol. Reactions of methanol on Pd particles have attracted considerable attention due to the activity of Pd catalysts with respect to important processes such as the synthesis or the partial and total oxidation of methanol (see, e.g., [23–26]). Interestingly, these catalysts show pronounced support, size, and promoter effects (see, e.g., [27–30]). Motivated by these observations, a number of studies on the reactivity of methanol have been have been performed under UHV conditions, both on Pd single crystals (see, e.g., [31–39]) and on Pd films [40]. Mechanistic issues regarding the decomposition on transition metal surfaces have been reviewed by Mavrikakis and Barteau [41], recently.

In a preceding study, we investigated mechanistic aspects and qualitative kinetic features of methanol decomposition on the alumina-supported Pd model catalyst, which is also used in this work [42]. Schematically, the key features are summarized in the reaction scheme displayed in Fig. 1: Methanol adsorbs molecularly on the Al_2O_3 support with desorption energies between 45 and 50 kJ mol^{-1}. On the Pd particles the adsorption energies are slightly higher, leading to reverse spillover and preferential adsorption on the particles. At low temperatures, breakage of the O–H bond on the Pd particles results in formation of methoxy species. Up to temperatures of 200 K, molecular methanol and methoxy species coexist and a rapid equilibrium between the two species is established. At higher temperatures decomposition proceeds via two competing pathways: The dominating pathway is dehydrogenation, leading to rapid formation

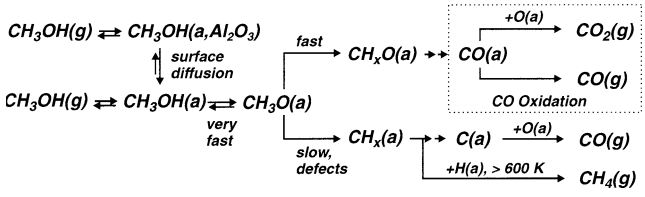

Fig. 1. Schematic reaction scheme for the decomposition and oxidation of methanol on a Pd/alumina model catalyst.

of CO. In a temperature-programmed reaction experiment, the reaction probability for dehydrogenation is found to depend sensitively on coverage (at low coverage the reaction rate is near unity). The CO produced in this process may either desorb ($\sim$ 480 K; see, e.g., [11]) or be oxidized to CO_2 in the presence of adsorbed oxygen ($\gtrsim$ 350 K, see, e.g., [20,22] and references therein). As a slow but competing pathway, we have recently identified C–O bond scission. Using CO as a probe molecule, we could show that C–O bond scission preferentially occurs at defect sites such as particle edges [43]. CH_x and carbon species produced via C–O bond scission can be removed by reaction with oxygen at moderate temperatures ($\gtrsim$ 400 K, [42]).

In this publication, we focus on the kinetics of methanol dehydrogenation to CO and subsequent oxidation to CO_2. It should be noted that at elevated temperatures ($>$ 300 K), adsorbed CO and oxygen are the only surface species that are present in substantial concentration. Thus, the surface kinetics is related to the well-known case of CO oxidation, with differences arising only from the fact that CO chemisorbs from the gas phase in the latter case, whereas it is formed via dehydrogenation in the case of methanol oxidation. We use this fact in two ways: (1) Experimentally, we perform equivalent measurements for both processes, CO and methanol oxidation. A direct comparison of the corresponding kinetic data allows a qualitative identification of key features and differences in the kinetics of both processes. (2) With respect to the microkinetic simulation, we start by modeling the simpler case of CO oxidation. In a second step, the kinetic parameters derived for the CO oxidation are then employed in a more complex kinetic model for methanol oxidation.

2. Experimental

All experiments were performed in a UHV molecular beam/surface spectroscopy apparatus at the Fritz-Haber-Institute (Berlin), which has been described in the literature recently [19]. The system offers the experimental possibility of up to three beams being crossed on the sample surface. In this study, CH_3OH (Merck, $>$ 99.8%), CO (AGA, $>$ 99.999%, further purified using a l-N_2 cold trap), and O_2 (AGA, $>$ 99.996%) beams were generated by two effusive beam sources based on multichannel arrays. Beam modulation is provided by a computer-controlled shutter located inside the second of two pumping stages of each beam source. To avoid artifacts due to nonhomogeneous coverage, the beam diameter was chosen so that it exceeded the sample surface for all IRAS experiments. Beam intensities and profiles were characterized as described in the literature [19]. In some experiments, a third source was used that generated a beam from a supersonic expansion (in this work CO or O_2 at backing pressures between 1.0×10^5 and 1.5×10^5 Pa).

For the calibration of IR absorption versus CO coverage, a sticking coefficient measurement (King and Wells method [44,45]) was performed at a sample temperature

of 300 K. For this purpose, the beam, generated by the supersonic source, was attenuated by a mechanical chopper to an intensity of 2.2×10^{13} molecules $cm^{-2}\,s^{-1}$ and the beam size was chosen to be smaller than the sample diameter. In an equivalent experiment but choosing a beam size larger than the sample, the IR spectra were continuously recorded as a function of CO exposure.

For the isotope exchange experiments a $^{12}CH_3OH$ and a $^{13}CH_3OH$ beam (Cambridge Isotope Laboratories, > 99%) of equal intensity were used. All reactivity measurements were performed via a quadrupole mass spectrometer (ABB Extrel) not in line of sight of the sample. The rate measurements for methanol oxidation to CO_2 were corrected for the background CO_2 signal produced in the vacuum chamber by subtracting a blind experiment performed on a Pd-free alumina sample. IR spectra were acquired at a spectral resolution of 2 cm^{-1} employing a vacuum FT-IR spectrometer (Bruker IFS 66v). A MIR polarizer was used to select the p-component of the IR light only. For the isotope exchange experiments, the data of several exchange cycles were accumulated to improve the signal to noise ratio.

Absolute turnover frequencies (TOF) as given in Section 3.6 were determined as follows: First, we determined the fraction of the flux emitted by the effusive source that impinged on the sample (note that the beam diameter was chosen larger than the sample and the beam profile was less well defined than for the supersonic beam source [19]). This was done by comparison of the background pressure in the scattering chamber, generated by the effusive beam sources and the supersonic beam source at equal beam intensity (as determined by the beam monitor [19]). For the supersonic source, the effusive part entering though the aperture of the last differential pumping stage was negligible and the beam profile could be determined exactly via the beam monitor. Once the total flux of CO or methanol into the vacuum chamber was known, we could calculate the absolute rate for conversion to CO_2 from the mass spectrum, taking into account the sensitivity factors for the different gases. Finally, the absolute TOF was determined using an estimate of the density of surface atoms derived from STM [10]. It should be pointed out that accuracy in the determination of both the reaction rates and the surface atom density was limited (with relative uncertainties typically on the order of 30% for both values). As a consequence, the uncertainty in the absolute values of the TOF was rather large (approximately 50%), whereas relative values were more reliable (see simulations in Section 3.6).

The alumina film was prepared by sputtering and annealing of a NiAl (110) single crystal, followed by repeated oxidation and annealing. The details of the oxidation procedure are given elsewhere [8,46]. Cleanliness and quality of the oxide film was checked via LEED (low energy electron diffraction) and AES (Auger electron spectroscopy). Before the experiment, Pd (> 99.9%) was deposited by evaporation from a rod (diameter 1 mm) using a commercial evaporator (Focus, EFM 3) based on electron bombardment (Pd coverage 2.7×10^{15} cm^{-2}, sample temperature 300 K). During deposition, the crystal was biased with a retarding voltage in order to prevent ions from being accelerated toward the sample (point defect creation). The evaporator flux was calibrated by a quartz microbalance prior to use. Before the reactivity experiments, the Pd particles were stabilized by oxygen and CO exposure as described previously [10,11].

3. Results and discussion

3.1. Structure of the $Pd/Al_2O_3/NiAl$ (110) model catalyst

Before we explore the kinetics of methanol decomposition and oxidation, we briefly reconsider the structure of the Pd particles on Al_2O_3/NiAl (110) employed in this study. More detailed structural information as well as data on adsorption properties can be found elsewhere [4,10]. Detailed information on the preparation and the structural properties of the Al_2O_3 model support is also given in the literature [7,8].

The structure of the Pd particles has recently been investigated by scanning tunneling microscopy (STM) and other methods (see [10] and references therein). It was found that the three-dimensional particles are characterized by an average size of 5.5 nm and contain about 3000 Pd atoms each, approximately 20% of which are located at the particle surface. The particle density corresponds to $1.0\ (\pm 0.2) \times 10^{12}$ cm^{-2}, resulting in about 20% of the support surface being covered by Pd particles. The majority of particles exhibit the morphology of well-shaped crystallites. These crystallites grow in (111) orientation and are predominantly terminated by (111) facets. Additionally, a small fraction of (100) facets are exposed.

For the reactivity experiments, the particles were stabilized prior to the experiment by extended oxygen exposure at elevated temperatures. Subsequently, surface oxygen was removed via reaction with CO, followed by thermal desorption of adsorbed CO. Details concerning the experimental procedure have been published previously [10,11]. Note that neither the particle shape nor the particle density is affected by this procedure.

3.2. Methanol oxidation to CO_2: molecular beam experiments

In order to systematically probe the kinetics of methanol oxidation, we perform a series of two-beam-experiments as illustrated in Fig. 2. The experimental setup is schematically depicted in Fig. 2b. A beam of oxygen and a beam of methanol, both of variable intensity are superimposed on the sample surface. We define the total effective pressure of oxygen and methanol at the sample position as

$$p_{\text{total}} = p_{\text{MeOH}} + p_{\text{O}_2} \quad \text{with } p_i = F_i (2\pi m_i kT)^{0.5} \qquad (1)$$

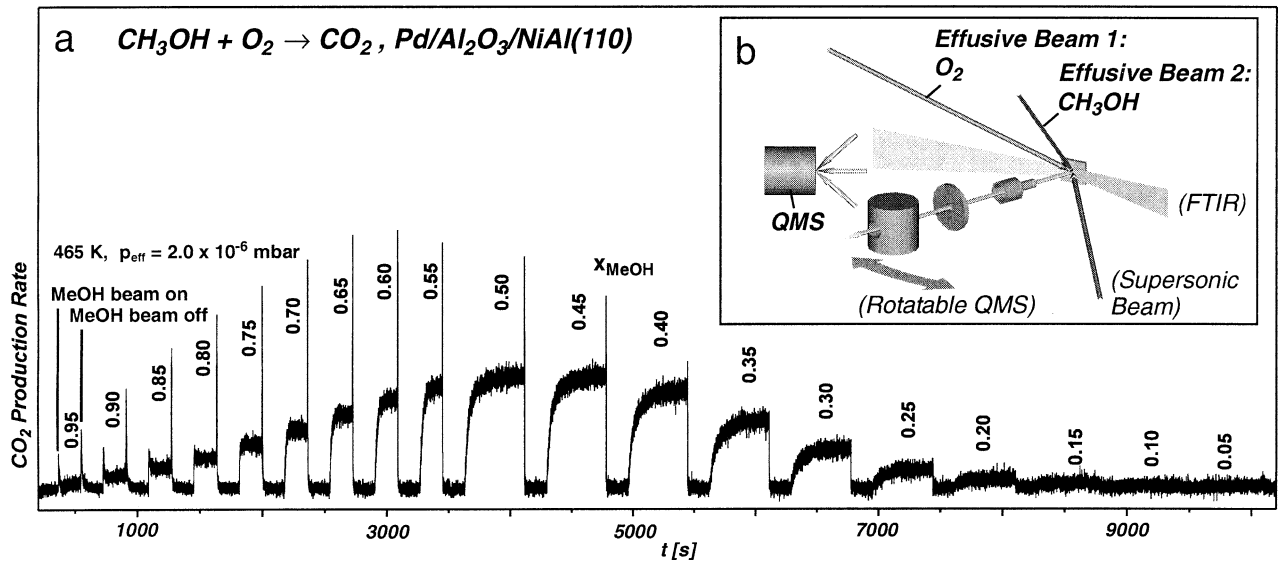

Fig. 2. (a) Transient response of the CO_2 production rate for a continuous O_2 beam and a modulated methanol beam impinging on the $Pd/Al_2O_3/NiAl$ (110) model catalyst as a function of the fraction of methanol x_{MeOH} in the gas flux ($T_s = 465$ K, $p_{total} = 2 \times 10^{-6}$ mbar); (b) schematic representation of the experimental setup.

and the fraction of methanol in the total flux impinging on the sample as

$$x_{MeOH} = \frac{F_{MeOH}}{F_{MeOH} + F_{O_2}}, \tag{2}$$

where F_i is the partial flux of reactant i at the sample position, m_i represents its molecular mass, and T_i is the temperature describing the velocity distribution (please note that for the experiments performed here $T_i = 300$ K, as no cooling of any degrees of freedom takes place in the effusive sources).

In a typical series of experiments as displayed in Fig. 2a, we record the rate of CO_2 formation while exposing the sample to a continuous beam of oxygen and a modulated beam of methanol. The methanol flux ratio x_{MeOH} is varied, whereas the total effective pressure p_{total} with both beams operating is kept constant. Previously, equivalent experiments have been performed for CO oxidation on the same model catalyst [20,21]. Again, it should be pointed out that adsorbed CO and oxygen are the only surface species present in considerable amounts for both reaction systems. Thus, we can directly attribute variations in the kinetics of CO_2 formation to differences in the decomposition kinetics of methanol as compared to the kinetics of CO adsorption.

From an experiment as shown in Fig. 2, two types of information can be extracted. First we obtain steady state reaction rates as a function of the methanol flux fraction x_{MeOH}. This type of experiment is combined with static in situ IRAS in order to correlate reaction rates with additional information on adsorbed surface species (see Section 3.3). The second type of information is contained in the transient behavior upon admission and termination of the methanol beam. Here, we use in situ time-resolved IRAS to monitor surface species and corresponding coverages (Section 3.4). Equivalent experiments have been performed for the CO oxidation previously, and we will use the corresponding results for comparison [20–22].

3.3. Methanol oxidation to CO_2: steady state kinetics

We start the discussion considering the CO_2 formation rates under steady state conditions. In Fig. 3a the reaction rate on $Pd/Al_2O_3/NiAl$ (110) is plotted as a function of the methanol fraction in the impinging flux x_{MeOH} and for different surface temperatures. A similar set of experiments for the CO oxidation is displayed in Fig. 3b.

The steady state data for the case of CO oxidation has been discussed in detail previously [20–22]. Briefly, we can distinguish between two reaction regimes, which we denote as *oxygen-rich* and *CO-rich*, respectively. Starting from oxygen-rich conditions (low x_{CO} values; x_{CO}: CO fraction in the impinging flux), the steady state is characterized by large oxygen and small CO coverages on the Pd particles. In this range, we observe a linear increase of the reaction rate with increasing CO flux. This linearity reflects the fact that preadsorbed oxygen has only a minor effect on the sticking probability of impinging CO. If we surpass a critical x_{CO} value, however, the rate starts to drop rapidly. This behavior is indicative of the transition to the CO-rich regime, which is characterized by an accumulation of chemisorbed CO on the surface of the Pd particles. The adsorbed CO inhibits dissociative adsorption of oxygen, giving rise to a rapid decrease in the oxidation rate with increasing x_{CO}. Upon raising the reaction temperature, the transition point, at which the system switches from oxygen-rich to CO-rich conditions shifts to larger x_{CO} values. This effect is due to the decreasing CO residence time and steady state coverages on the surface.

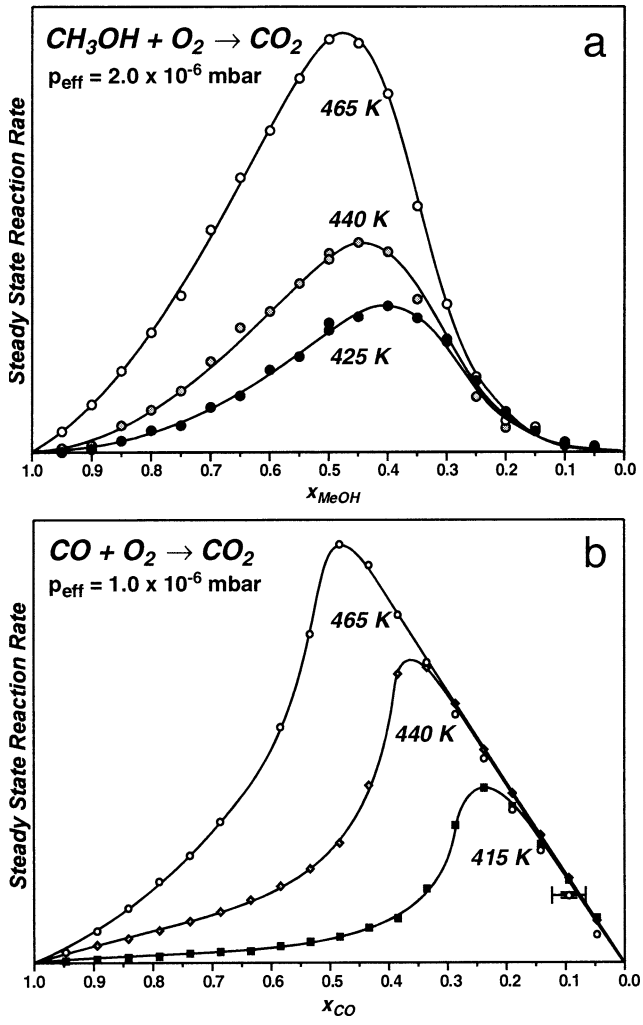

Fig. 3. Steady state reaction rates on the $Pd/Al_2O_3/NiAl$ (110) model catalyst as a function of the fraction of methanol x_{MeOH} in the impinging gas flux and the surface temperature (a) for the total oxidation of methanol ($p_{total} = 2 \times 10^{-6}$ mbar); (b) for the CO oxidation ($p_{total} = 1 \times 10^{-6}$ mbar).

Comparing the steady state reaction rates for methanol oxidation to the corresponding rates for CO oxidation (Figs. 3a and 3b), we can identify the same two regimes for the methanol reaction system, i.e., a flux region in which the surface is predominantly covered by oxygen ($0 < x_{MeOH} < 0.45$) and a region in which it is predominantly covered by CO ($0.45 < x_{MeOH} < 1$). The steady state plots, however, reveal several pronounced differences between the two processes: (1) In contrast to the CO case, CO_2 production from methanol is strongly suppressed at high oxygen fluxes and increases nonlinearly as a function of x_{MeOH}. (2) For large methanol fractions x_{MeOH}, the decrease in the reaction rate (i.e., the CO poisoning of the surface) appears to be less pronounced than for the CO oxidation case. (3) The x_{MeOH} value at which the reaction rate reaches its maximum shows only slight shifts as a function of temperature.

In order to explore the differences between the two oxidation processes, we have performed IRA spectroscopy (CO stretching frequency region) under reaction conditions. A typical set of experiments is displayed in Figs. 4a and 4b. Simultaneously with the rate measurements (Fig. 4a), we record an IR spectrum for every set of reaction conditions after the corresponding steady state is fully established (Fig. 4b). We observe a main feature at 1905 cm^{-1} (1), a broader absorption at 1830 cm^{-1} (2), and in some cases a very weak feature at approximately 2050 cm^{-1} (3). Previously, the origin of these bands has been discussed and they have been assigned to (1) CO adsorbed at hollow sites on (111) facets superimposed with (100) facets, defects and bridge sites, (2) CO adsorbed at hollow sites on (111), and (3) CO linearly adsorbed on (111) facets and at defects (see, e.g., [9,47,48] and references therein).

A comparison of the integral absorption in the CO region during CO and methanol oxidation is shown in Figs. 4c and 4d. Again we find clear differences for the two reaction systems: In the CO case, we observe a linear increase in the CO absorption signal with x_{CO} at low CO flux, a sharp increase in absorption upon transition to the CO-rich regime, and a nearly constant value at large x_{CO}. For methanol oxidation, on the other hand, the CO absorption signal remains below the detection limit for $x_{MeOH} < 0.2$. For higher x_{MeOH} values it increases smoothly without showing the pronounced step-like characteristics of CO oxidation.

With respect to the interpretation of the IR absorption data, it should be noted that in IRAS there is no simple relationship between integral absorption and the surface coverage (see, e.g., [49]). The problem can be surmounted by suitable calibration procedures, as discussed in Section 3.4. Here, we restrict ourselves to qualitative information, which is directly evident from the absorption data.

From both rate measurements and in situ IRAS it is apparent that preadsorbed oxygen has a strongly inhibiting effect on the dehydrogenation rate of methanol. On a molecular level, several contributions may be invoked as a possible origin of this inhibition effect, such as site blocking in the adsorption dissociation process, variations of the activation barrier for dissociation and desorption induced by preadsorbed oxygen, or the formation of oxygen islands with specific reaction properties. With respect to the first point, previous adsorption measurements have shown that preadsorbed oxygen does not prevent methanol adsorption and methoxy formation on the Pd particles at low temperatures, but still reduces the dehydrogenation probability [42]. Similar inhibiting effects have been found for methanol decomposition other surfaces, such as Mo (110) [50] or Cu (110) [51]. In the latter case it was shown that oxygen forms islands with only very few centers being active with respect to methanol. We will come back to this point in connection with the microkinetic modeling discussed in Section 3.6.

3.4. Methanol oxidation to CO_2: transient kinetics

After discussing the basic features of the steady state reaction behavior, we consider the transient rates of CO_2

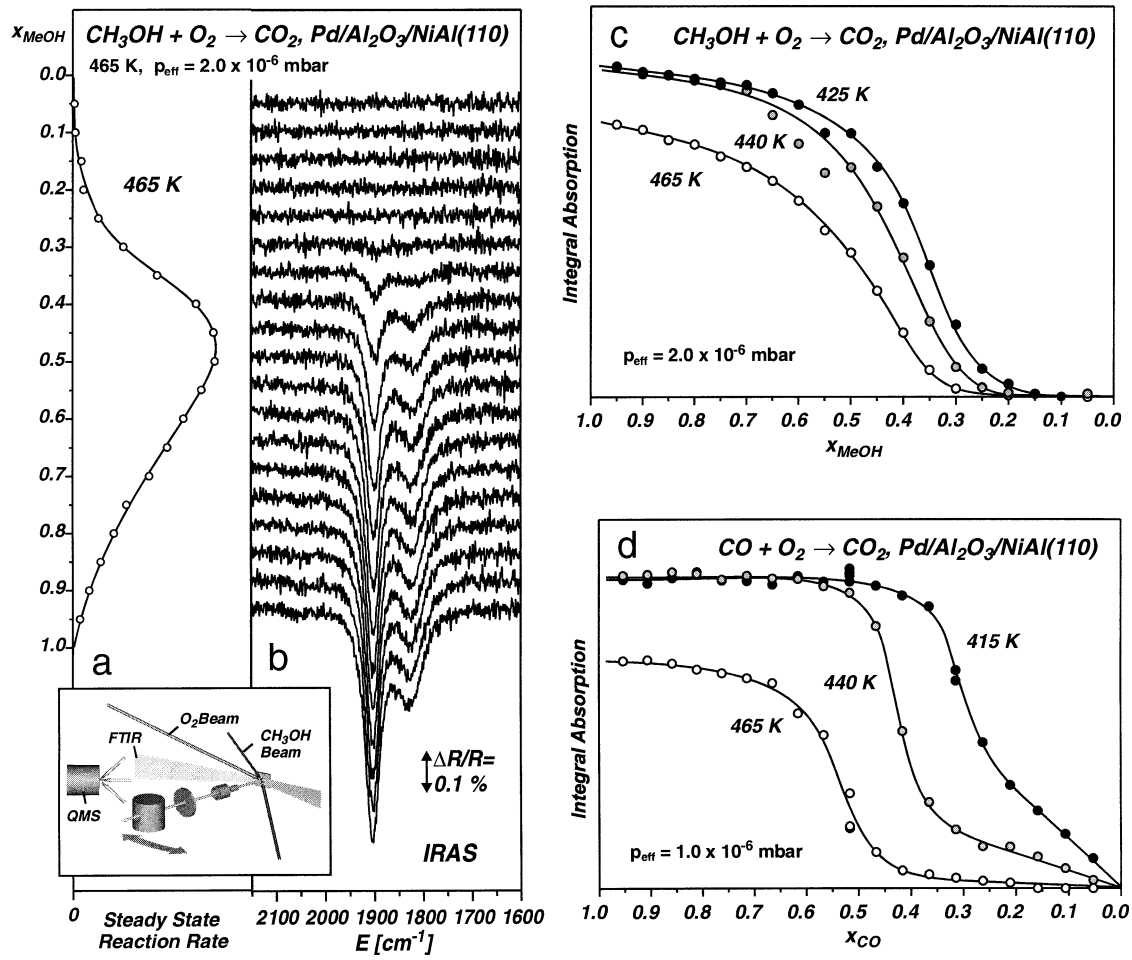

Fig. 4. (a) Steady state CO_2 production rates and (b) static in situ IR reflection absorption spectra of CO on the $Pd/Al_2O_3/NiAl$ (110) model catalyst during methanol oxidation as a function of the fraction of methanol x_{MeOH} in the impinging gas flux ($T_s = 465$ K); (c) integral absorption in the CO stretching frequency region during methanol oxidation ($p_{total} = 2 \times 10^{-6}$ mbar) and (d) during CO oxidation, for comparison ($p_{total} = 1 \times 10^{-6}$ mbar).

formation in more detail. In Fig. 5 we make a direct comparison between the transient rates of CO oxidation and methanol total oxidation under both oxygen-rich and CO/methanol-rich conditions.

The transient behavior for the CO oxidation (Fig. 5c) has been discussed elsewhere [20,22,52]. Briefly, the two reaction regimes, CO-rich and O-rich, are connected to two characteristic types of transients: (1) Under O-rich conditions (lower trace in Fig. 5c), an instantaneous increase in the reaction rate (on the timescale of the experiment) is observed upon admission of a CO beam to the oxygen saturated surface, followed by a slower increase toward the steady state rate. The behavior was rationalized by the presence of a CO precursor state, which is rapidly populated and from which a chemisorption state can be reached. The probability of chemisorption (rapidly followed by reaction and desorption of CO_2) slightly depends on the oxygen coverage, giving rise to the slower part of the transient increase. Upon termination of the CO beam, the reaction rate drops rapidly, as the remaining low coverage of CO is rapidly consumed in the reaction. (2) Different behavior is found under CO-rich conditions (see Fig. 5c, upper trace). Again we observe an instantaneous rise in the CO_2 production upon exposure of the oxygen saturated surface to the CO beam, followed by a slower increase (see also [20]). Subsequently, the reaction rate drops again due to the accumulation of CO and the connected inhibition of oxygen adsorption (see discussion in Section 3.3). The steady state is characterized by high CO and low O coverages. Once the CO beam is terminated again, the reverse process occurs. The reaction rate increases as a result of the decreasing CO coverage (leading to an increasing oxygen chemisorption probability) and gives rise to a CO_2 formation peak.

At this point it should be noted that for the CO oxidation on Pd particles a third type of transient is observed upon termination of the beam in a transition region between the CO- and oxygen-rich regimes, which is characterized by a minimum in the reaction rate [20,21,53,54]. This type of behavior is related to the presence of defects and surface heterogeneities. For a detailed discussion we refer to the literature [20,22].

Comparing the transient CO_2 production for methanol oxidation (Fig. 5b) to the CO oxidation case, drastic differences are observed: (1) Under oxygen-rich conditions, we

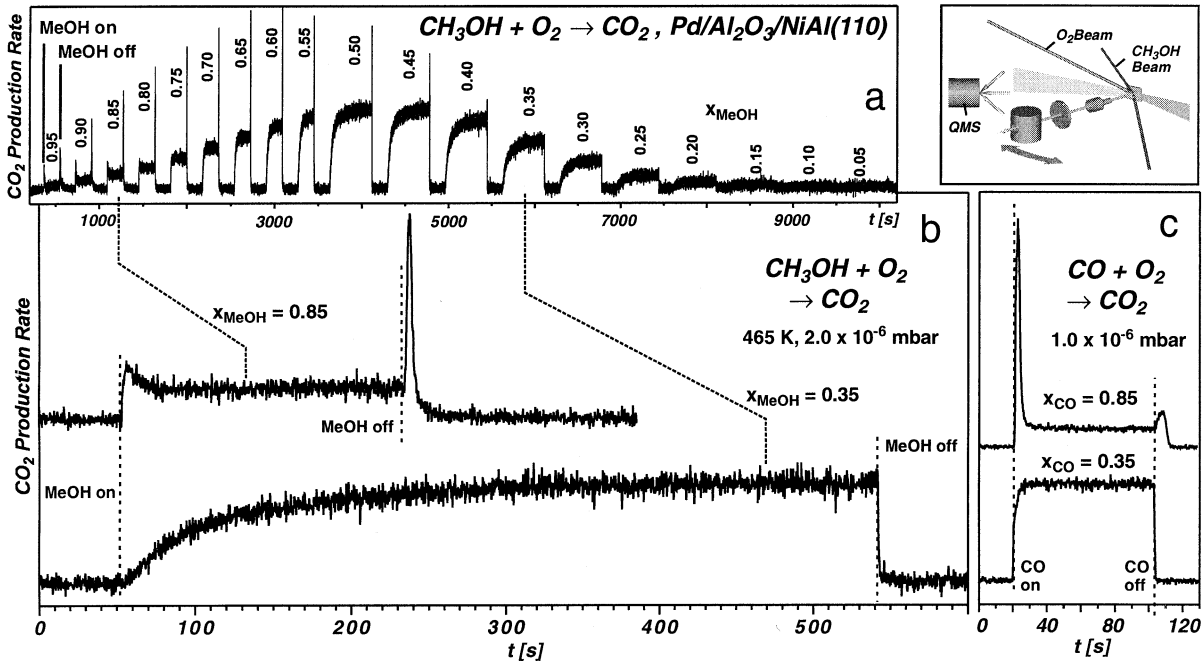

Fig. 5. (a) Transient CO_2 production rates as a function of the fraction of methanol x_{MeOH} in the gas flux and (b) close-up of two characteristic transients ($T_s = 465$ K, $p_{total} = 2 \times 10^{-6}$ mbar); (c) transient CO_2 production rates for CO oxidation, for comparison ($T_s = 465$ K, $p_{total} = 1 \times 10^{-6}$ mbar).

observe no instantaneous increase in the reaction rate upon exposure to the methanol beam. Instead, the reaction rate initially remains below the detection limit and subsequently increases slowly towards the steady state level. The timescale on which the steady state level is reached (approximately 300 s for the transient displayed in Fig. 5b) is typically an order of magnitude slower than for the CO oxidation. Upon termination of the methanol beam, the reaction rate drops rapidly, showing that the steady state coverage of CO is low under these conditions. (2) Under methanol-rich conditions the main difference is related to the initial transient CO_2 peak upon admission of the methanol beam. This peak is strongly attenuated in the case of the methanol oxidation. Still, the intense CO_2 peak, which appears upon termination of the beam, clearly demonstrates that the steady state is characterized by a high CO coverage. In particular, it is noteworthy that for a broad range of conditions no transient maximum appears at all upon admission of the methanol beam, whereas a pronounced CO_2 peak is observed upon termination (see Figs. 5a and 2). In contrast to this the appearance of the two transient maxima is typically connected in the case of the CO oxidation (and indicative of the CO-rich reaction regime; see discussion above). Last but not least, the transient transition behavior mentioned above (characterized by a minimum in the reaction rate upon termination of the CO beam; see [20,21,53,54]) is not found for the methanol case.

In order to obtain additional kinetic information under transient conditions, we have performed TR-IRA spectroscopy correlated with reaction rate measurements. A typical experiment is displayed in Fig. 6. We focus on conditions ($x_{MeOH} = 0.5$) under which the CO_2 production shows an unusually slow transient increase and no maximum in the reaction rate upon admission of the methanol beam (although substantial CO coverages are built up in the steady state, as indicated by the appearance of the CO peak upon termination of the methanol beam). For comparison the reverse experiment, using a continuous methanol beam and a modulated O_2 beam, is also displayed in Fig. 6a. The IRA spectra are displayed in Fig. 6b, which were recorded in the transient region as a function of time. As expected we find a slow increase in the absorption signal starting from the oxygen-precovered system (modulated methanol beam) and a rapid decrease starting from the CO-precovered system (modulated oxygen beam).

The integral absorption corresponding to the spectra displayed in Fig. 6 b is shown in Fig. 7. As discussed before, no general relationship is valid in IRAS, which allows us to convert this type of data into coverage. In order to circumvent this problem, we perform a coverage calibration by combining a sticking coefficient measurement and TR-IRA spectroscopy. The calibration experiment is performed at a sample temperature of 300 K, assuming a saturation coverage of 0.5 at 300 K (see, e.g., [55]). The result is displayed in Fig. 7b. As observed previously for other systems (see, e.g., [49] and references therein), the absorption increases rapidly with coverage in the low-coverage regime, whereas at high coverage the dependence becomes much weaker.

We use this calibration curve to convert absorption data into coverage. The calculated CO coverage θ_{CO} in the transient region is displayed in Fig. 7c. Moreover, we can calculate the rate of CO accumulation on the surface, $d\theta_{CO}/dt$, which is shown in Fig. 7d.

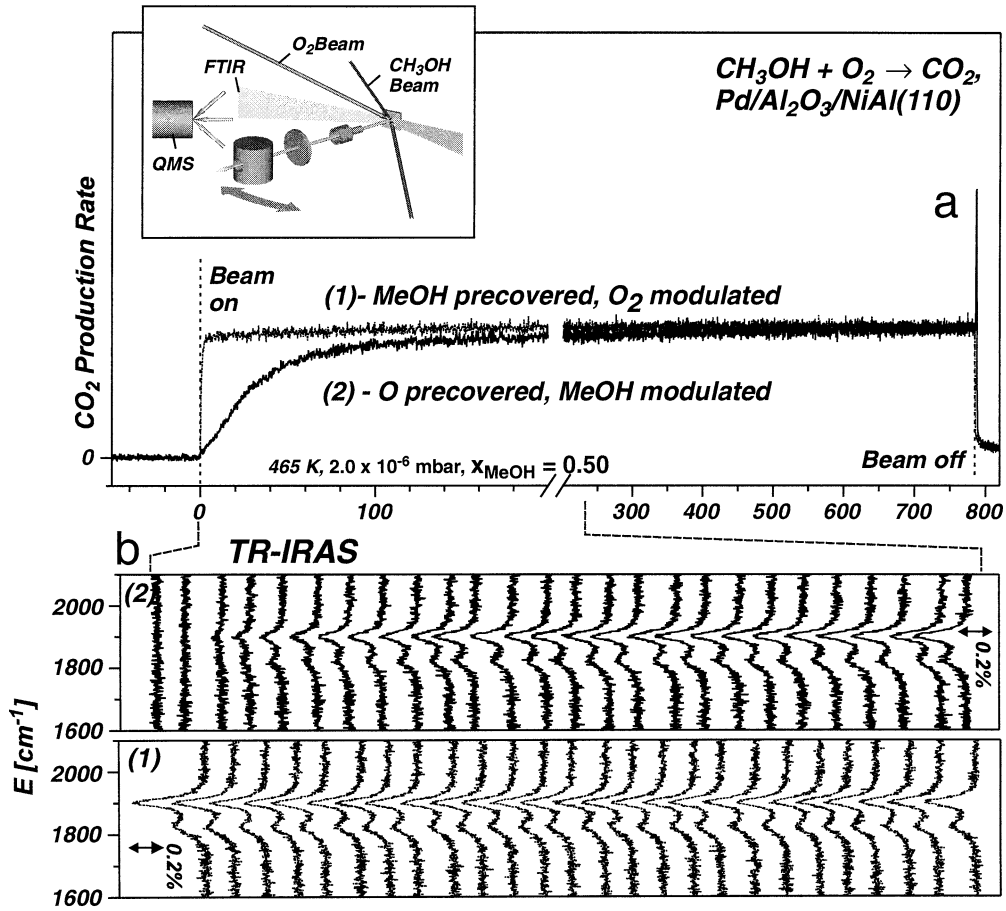

Fig. 6. (a) Transient CO_2 production rates and (b) corresponding TR in situ IR reflection absorption spectra of CO during methanol oxidation on the $Pd/Al_2O_3/NiAl$ (110) model catalyst ($T_s = 465$ K, $p_{total} = 2 \times 10^{-6}$ mbar); (1) continuous methanol beam, modulated oxygen beam; (2) modulated methanol beam, continuous oxygen beam.

The transient behavior of the CO coverage derived via TR-IRAS shows the same general behavior as the reaction rate measurements. Starting from a CO precovered surface, the rate of CO formation shows an immediate increase on the timescale of the experiment and the steady state is reached rapidly. Starting from an oxygen precovered surface, however, the initial reaction rate on the fully oxygen-saturated surface is low, but increases once adsorbed oxygen is consumed in the course of the reaction. An equivalent behavior was found for the transient rate measurements, where no immediate CO_2 production was observed upon admission of the methanol beam (Fig. 5). Both observations illustrate the strongly inhibiting effect of a saturated oxygen layer on the dehydrogenation process. This inhibition effect may contribute to the differences in the transient reaction rates for methanol oxidation, i.e., the much slower increase in the rate and the attenuation of the transient CO_2 peak upon exposure to the methanol beam. It remains the question, how the inhibition effect arises in detail. We will come back to this questions in connection with the kinetic simulations in Section 3.6. Moreover, we have to invoke the possible formation of carbon and its influence on the transient reaction rates. Recently, we have shown that carbon can be accumulated under conditions of low oxygen flux and specifically blocks particle defect sites [42,43]. Thus, the fact that the transient behavior in the transition region between O-rich and CO-rich steady states (transient minimum in the reaction rate; see [20–22]), which sensitively depends on the presence of surface defects, is suppressed for methanol total oxidation may be due to a blocking of these defect sites by carbon species.

3.5. Methanol dehydrogenation to CO: isotope exchange experiments

So far we have exclusively investigated the kinetics of methanol total oxidation, i.e., the rate of CO_2 formation. In general, we are, however, more interested in the kinetics of the dehydrogenation process itself, which in the absence of oxygen may also lead to CO as a product. Thus, it would be desirable to detect both the rate of CO and CO_2 formation in steady state and transient measurements (Figs. 2, 3, and 5). Unfortunately, we are facing the experimental difficulty that CO represents a major fragmentation product of methanol in the ionizer of a quadrupole mass spectrome-

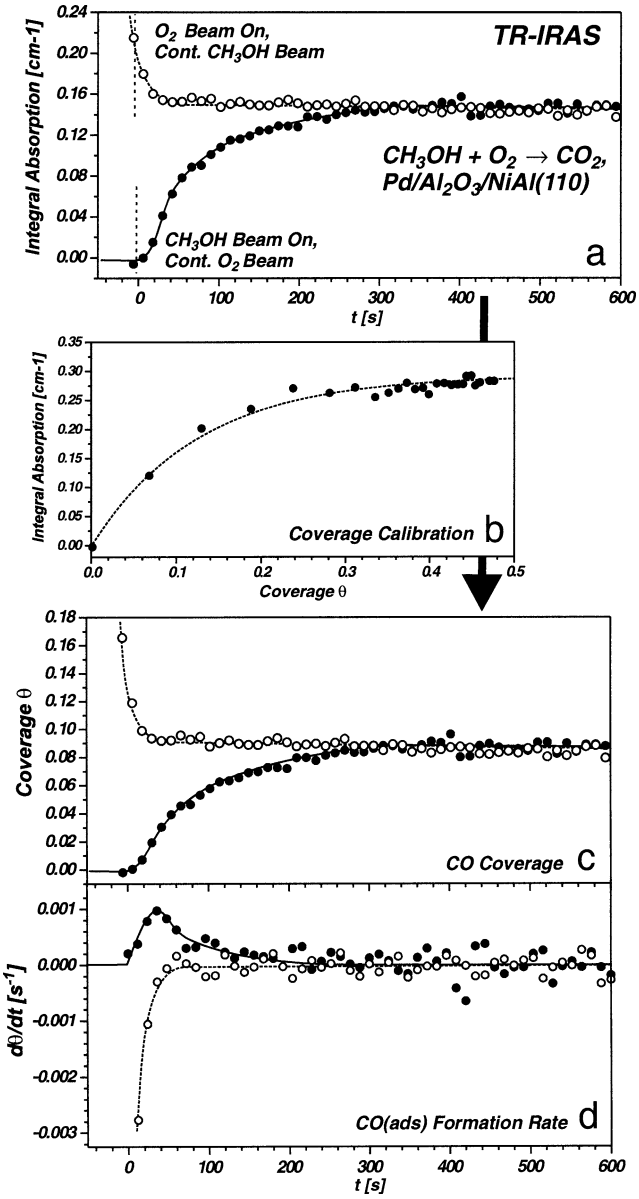

Fig. 7. (a) Integral absorption corresponding to the spectra displayed in Fig. 6. Open symbols: continuous methanol beam, modulated oxygen beam; solid symbols: modulated methanol beam, continuous oxygen beam. (b) Integral absorption in the CO stretching frequency region as a function of CO coverage. (c) CO coverage in the transient region as calculated from the TR-IRA spectra. (d) Derivative of the CO coverage in the transient region.

ter (QMS). The resulting high background level prevents direct measurements of the CO production via a QMS.

We can, however, circumvent the problem by performing an isotope exchange/TR-IRAS experiment as displayed in Fig. 8. Two beam sources of equal intensity are superimposed on the sample, one supplying $^{12}CH_3OH$ and the other isotopically labeled $^{13}CH_3OH$. We switch between both beams using beam shutters, synchronized with the IR data acquisition. Simultaneously, oxygen is supplied via a third beam source. The time constant of exchange between the adsorbed dehydrogenation products ^{12}CO and ^{13}CO is monitored via TR-IRAS and directly yields the total rate constant for CO removal from the surface, i.e., the sum of desorption of CO and oxidation to CO_2. If the total CO coverage is known (i.e., from the IR absorption calibrated as described in Section 3.5), we can also calculate the absolute rates of CO and CO_2 formation. In order to minimize the influence of carbon produced by C–O bond scission during the exchange experiment, experiments with low oxygen flux were performed on freshly prepared samples [42,43].

An example for the type of experimental data obtained is displayed in Fig. 8a ($x_{\mathrm{MeOH}} = 1$, $T_{\mathrm{surface}} = 465$ K). We switch between two methanol beams, providing an effective pressure at the sample position of 2×10^{-6} mbar, and record IR spectra with a temporal resolution of 240 ms. Thus, we can follow the exchange between ^{12}CO, characterized by an absorption band at 1900 cm^{-1} with a shoulder at 1840 cm^{-1} (at the sample temperature of 465 K), and ^{13}CO, characterized by an absorption band at 1860 cm^{-1} and a shoulder at 1800 cm^{-1}. In order to quantify the time constant of exchange, we determine the mean absorption energy in the CO stretching frequency region. The result is displayed in Fig. 8b for different surface temperatures ($x_{\mathrm{MeOH}} = 1$). Within experimental accuracy, the absorption energy follows an exponential behavior and the characteristic time constants for exchange τ_{exc} are determined from a fit of this data.

Note that for $x_{\mathrm{MeOH}} = 1$, τ_{exc} is determined by CO desorption exclusively (with respect to the possible determination of desorption parameters from this type of experiment, however, it should be pointed out that the steady state surface coverage und thus the repulsive adsorbate interaction varies as a function of temperature). In the presence of oxygen, however, both desorption and oxidation may contribute to the CO removal rate. Here, we are mainly interested in the influence of oxygen on the dehydrogenation kinetics. The results of corresponding experiments are summarized in Fig. 8c, showing τ_{exc} as a function surface temperature and methanol fraction x_{MeOH} ($p_{\mathrm{total}} = 2 \times 10^{-6}$ mbar). It is found that there is only a weak dependence of τ_{exc} on the oxygen flux applied. This implies that there is no pronounced inhibition of dehydrogenation under oxygen-poor conditions. Instead, the reaction proceeds with similar kinetics, but with CO as the main product, whereas under oxygen-rich conditions the majority of CO is oxidized to CO_2.

3.6. Microkinetic modeling

In order to approach a microkinetic modeling of the methanol decomposition process, we simplify the reaction scheme in Fig. 1 according to previous experimental findings [42,43]. The simplified kinetic scheme is displayed in Fig. 9.

The first step is the adsorption of molecular methanol, which may be modified by trapping on the support and surface diffusion. As the interaction with the support is weak [42], however, this process is fast on the timescale of the reaction and we may include the trapping effect by

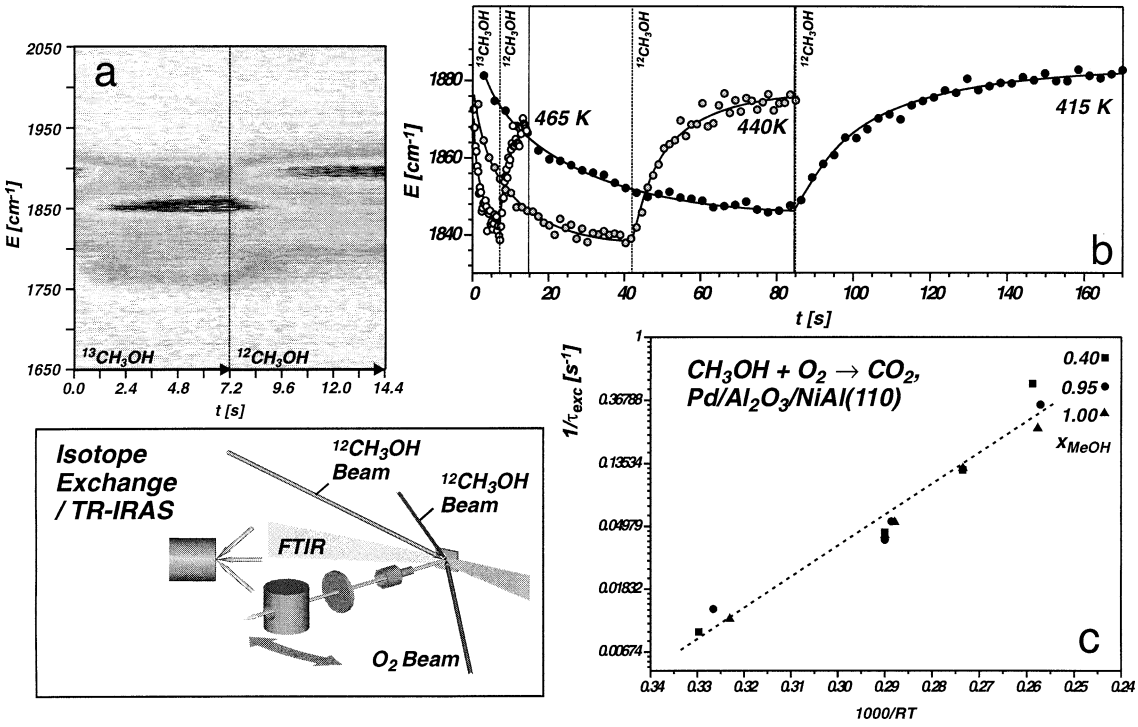

Fig. 8. Isotope exchange experiment for determination of the methanol decomposition rate on $Pd/Al_2O_3/NiAl$ (110) under steady state conditions; (a) temporal evolution of absorption in the CO stretching frequency region upon exchange between $^{12}CH_3OH$ and $^{13}CH_3OH$; (b) temporal response of the mean absorption energy in the CO stretching region for different surface temperatures ($x_{MeOH} = 1$); (c) time constant for isotope exchange for different surface temperatures and fractions of methanol x_{MeOH} in the impinging gas flux ($p_{total} = 2 \times 10^{-6}$ mbar).

introducing an effective sticking coefficient $S_{i,\mathrm{eff}}$ for every species i. Subsequently, the adsorbed methanol undergoes partial dissociation to methoxy and a fast equilibrium is established between the two species [42]. Consequently, the methanol/methoxy system is treated as a single intermediate, the reaction probability of which may depend on the actual surface coverages. Note that under the reaction conditions applied in the total oxidation experiments ($T_{\mathrm{surface}} > 400$ K), dehydrogenation is fast and consequently the steady state coverages of methoxy and methanol are extremely low. Moreover, it should be pointed out that the lifetime of all further intermediates of dehydrogenation is even shorter, so that in the kinetic scheme the multiple step dehydrogenation process can be represented by a single step.

As products of dehydrogenation we may obtain CO as well as adsorbed hydrogen or hydroxyl. The desorption of hydrogen from Pd is again fast under our conditions (in a TPD (temperature programmed desorption) experiment, two desorption features are observed at approximately 280

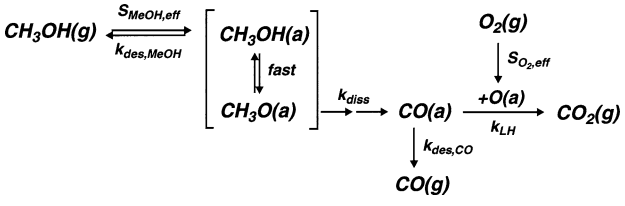

Fig. 9. Simplified reaction diagram for the kinetic simulation of methanol oxidation on the $Pd/Al_2O_3/NiAl$ (110) model catalyst.

and 310 K for Pd particles of 5 nm size [56]). Desorption of H_2O could not be detected under the conditions applied here, however, formation of small amounts of water cannot be excluded either due to the large background level at 18 amu in the presence of methanol. Following these observation we omit the desorption and reaction of hydrogen/OH in the kinetic model, but it has to be pointed out that oxygen consumption due to possible formation of a certain amount of water might lead to slight modifications of the reaction rates under oxygen-rich conditions.

The CO produced in the reaction can either desorb or react with adsorbed oxygen to form CO_2, which itself desorbs rapidly. Under the conditions employed here, CO and O are the only surface species present in large concentrations. Taking into account this point, it is tempting to follow a two-step strategy: First, we consider the kinetics of CO oxidation as a simple and well-known reaction system. From a fit of a corresponding kinetic model to the experimental data, we obtain several kinetic parameters, which, in a second step, can be used in kinetic model for the methanol oxidation. The remaining parameters are adjusted in a fitting procedure to reproduce the kinetic data for the methanol system.

The CO oxidation is treated as previously described in the literature [20]. The differential equations describing the time evolution of the CO coverage θ_{CO}, the O coverage θ_{O}, and the reaction rate $r_{\mathrm{CO_2}}$ per active site (TOF) are

$$\frac{\mathrm{d}\theta_{\mathrm{CO}}}{\mathrm{d}t} = S_{\mathrm{CO,eff}}\frac{F_{\mathrm{CO}}}{n_{\mathrm{Pd}}} - k_{\mathrm{des}}^{\mathrm{CO}}\theta_{\mathrm{CO}} - k_{\mathrm{LH}}\theta_{\mathrm{O}}\theta_{\mathrm{CO}}, \tag{3}$$

$$\frac{\mathrm{d}\theta_{\mathrm{O}}}{\mathrm{d}t} = 2S_{\mathrm{O_2,eff}}\frac{F_{\mathrm{O_2}}}{n_{\mathrm{Pd}}} - k_{\mathrm{LH}}\theta_{\mathrm{O}}\theta_{\mathrm{CO}}, \tag{4}$$

$$r_{\mathrm{CO_2}} = k_{\mathrm{LH}}\theta_{\mathrm{O}}\theta_{\mathrm{CO}}, \tag{5}$$

with F_{CO} and $F_{\mathrm{O_2}}$ representing the fluxes of CO and O_2. n_{Pd} is the density of Pd surface atoms, and $S_{\mathrm{CO,eff}}$ and $S_{\mathrm{O_2,eff}}$ are the effective sticking coefficients, described as

$$S_{\mathrm{CO,eff}} = S^0_{\mathrm{CO,eff}}\left(1 - C_{T_\mathrm{s}}\frac{\theta_{\mathrm{O}}}{\theta^{\max}_{\mathrm{O}}} - \frac{\theta_{\mathrm{CO}}}{\theta^{\max}_{\mathrm{CO}}}\right)^{a_{\mathrm{CO}}}, \tag{6}$$

$$S_{\mathrm{O_2,eff}} = S^0_{\mathrm{O_2,eff}}\left(1 - \frac{\theta_{\mathrm{O}}}{\theta^{\max}_{\mathrm{O}}} - \frac{\theta_{\mathrm{CO}}}{\theta^{\max}_{\mathrm{CO}}}\right)^{a_{\mathrm{O_2}}}. \tag{7}$$

Here, $S^0_{\mathrm{CO,eff}}$ and $S^0_{\mathrm{O_2,eff}} = S^{0,T_\mathrm{s}=0}_{\mathrm{O_2,eff}} - 7.4\times10^{-4}\cdot T_\mathrm{s}$ (see [20,55]) are the zero coverage sticking coefficients (including support trapping effects); $\theta_i^{\max}$ stands for the saturation coverage, with $\theta^{\max}_{\mathrm{CO}} = 0.5$ and $\theta^{\max}_{\mathrm{O}} = 0.25$ (see [20,57]), a_i is the number of surface sites involved in the process i (in a simple Langmuir model); and C_{T_s} describes the influence of adsorbed oxygen on the chemisorption of CO [20, 52,58]. The temperature dependence of the rate constants for CO desorption $k^{\mathrm{CO}}_{\mathrm{des}}$ and the Langmuir–Hinshelwood reaction step k_{LH} is described as

$$k^{\mathrm{CO}}_{\mathrm{des}} = \nu^{\mathrm{CO}}_{\mathrm{des}}\exp\left(-\frac{E^{\mathrm{CO}}_{\mathrm{des}}}{kT_\mathrm{s}}\left(1 - \alpha_{\mathrm{CO}}\frac{\theta_{\mathrm{CO}}}{\theta^{\max}_{\mathrm{CO}}}\right)\right), \tag{8}$$

$$k_{\mathrm{LH}} = \nu_{\mathrm{LH}}\exp\left(-\frac{E_{\mathrm{LH}}}{kT_\mathrm{s}}\right). \tag{9}$$

In these equations, $E^{\mathrm{CO}}_{\mathrm{des}}$ and E_{LH} are the activation energies for desorption and reaction, $\nu^{\mathrm{CO}}_{\mathrm{des}}$ and ν_{LH} are the corresponding preexponential factors, and α_{CO} describes the coverage dependence of the desorption energy.

Previously, we have performed kinetic simulations of CO oxidation under both transient and steady conditions, which were mainly based on single-crystal experimental values for sticking coefficients, activation energies, and prefactors [20,22]. These simulations were able to reproduce the experiments on a semiquantitative basis. Quantitative agreement cannot be expected, because of large uncertainties in the experimental values and possible deviations of the supported particle system from the single-crystal behavior. Starting from the values of the previous simulation, we have fitted the described kinetic model to the experimental steady state rates. The fit was performed under the constraint that the absolute TOF values contain large uncertainties, but the relative values (i.e., the shape of the curves displayed in Fig. 3b) are reliable. Additionally, only those sets of parameters were considered, which also provide a good description of the experimental transient behavior.

A typical fit is displayed in Fig. 10a. The corresponding parameters are given in Table 1. We find that the steady state reaction rates are well reproduced by the model. Moreover, the calculated turnover frequencies are found to fall into the same range as the experimental values, although not used as a fitting criterion. In Fig. 10b we compare a typical experimental transient under CO-rich conditions to the

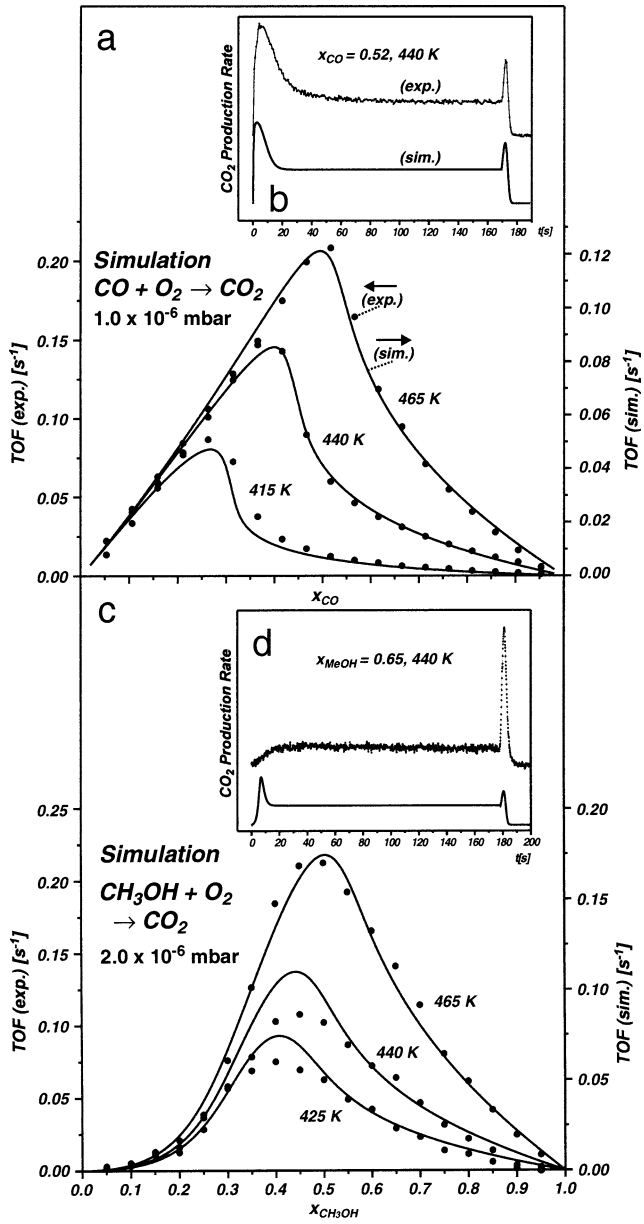

Fig. 10. (a) Comparison between simulated and experimental steady state reaction rates for the CO oxidation on $Pd/Al_2O_3/NiAl$ (110) as a function of surface temperature and methanol fraction x_{MeOH} in the impinging flux; (b) comparison of simulated and experimental transients for the CO oxidation; (c) comparison between simulated and experimental steady state reaction rates for the total oxidation of methanol; (d) comparison of simulated and experimental transients for methanol total oxidation.

simulation. Again, the general behavior, the timescale of the transient response, and the relative intensity of the transient peaks are found to be well reproduced. We conclude that, in spite of its simplicity, the model provides a satisfactory quantitative description of the CO oxidation kinetics, under both steady state and transient conditions.

In the next step we set up a kinetic model for the oxidation methanol, starting from the CO oxidation system and adding adsorption, desorption, and dehydrogenation steps for methanol/methoxy. In this way, we obtain the

Table 1
Parameters used in the microkinetic simulation of the CO and methanol oxidation

Process	Parameter	CO oxidation	Methanol oxidation
CO desorption	ν_{CO} [s^{-1}]	3.2×10^{13}	3.2×10^{13}
	E_{des}^{CO} [kJ mol^{-1}]	135	135
	α_{CO}	0.15	0.15
CO adsorption	$S_{CO,eff}^{0}$	0.7	
	C_{T_s}	0.4	
	θ_{CO}^{max}	0.5	0.5
O_2 adsorption	$S_{O_2,eff}^{0,T_s=0}$	1.0	1.0
	a_{O_2}	2	2
	θ_{O}^{max}	0.25	0.25
Methanol adsorption	$S_{MeOH,eff}^{0}$		0.6
	a_{MeOH}		1
	ε_O		0
	ε_{CO}		1
	θ_{MeOH}^{max}		1
Methanol desorption	ν_{des}^{MeOH} [s^{-1}]		1×10^{12}
	E_{des}^{MeOH} [kJ mol^{-1}]		50
	γ_O		0
	γ_{CO}		0
CO oxidation	ν_{LH} [s^{-1}]	6.4×10^{8}	6.4×10^{8}
	E_{LH} [kJ mol^{-1}]	66	66
Methanol dehydrogenation	ν_{dehyd} [s^{-1}]		8×10^{12}
	E_{dehyd} [kJ mol^{-1}]		45
	a_{dehyd}		1
	β_O		−0.3
	β_{CO}		−0.25

following set of differential equations:

$$\frac{d\theta_{MeOH}}{dt} = S_{MeOH,eff}\frac{F_{MeOH}}{n_{Pd}} - k_{des}^{MeOH}\theta_{MeOH} - k_{dehyd}\theta_{MeOH}\theta_{free}^{a_{dehyd}}, \quad (10)$$

$$\frac{d\theta_{CO}}{dt} = k_{dehyd}\theta_{MeOH}\theta_{free}^{a_{dehyd}} - k_{des}^{CO}\theta_{CO} - k_{LH}\theta_O\theta_{CO}, \quad (11)$$

$$\frac{d\theta_O}{dt} = 2S_{O_2,eff}\frac{F_{O_2}}{n_{Pd}} - k_{LH}\theta_O\theta_{CO}, \quad (12)$$

$$r_{CO_2} = k_{LH}\theta_O\theta_{CO}. \quad (13)$$

Here, θ_{free} is the fraction of free sites,

$$\theta_{free} = 1 - \frac{\theta_O}{\theta_O^{max}} - \frac{\theta_{CO}}{\theta_{CO}^{max}} - \frac{\theta_{MeOH}}{\theta_{MeOH}^{max}}, \quad (14)$$

and a_{dehyd} is the number of additional sites required for the dehydrogenation step. The effective methanol sticking coefficient, $S_{MeOH,eff}$, is modeled as

$$S_{MeOH,eff} = S_{MeOH,eff}^{0}\left(1 - \varepsilon_O\frac{\theta_O}{\theta_O^{max}} - \varepsilon_{CO}\frac{\theta_{CO}}{\theta_{CO}^{max}} - \varepsilon_{MeOH}\frac{\theta_{MeOH}}{\theta_{MeOH}^{max}}\right)^{a_{MeOH}}, \quad (15)$$

with the parameters ε_i describing the inhibiting effects of different surface species on the adsorption of methanol and a_{MeOH} representing the number of sites required by adsorbed methanol. Adsorption experiments suggest coadsorption of methanol and oxygen at low temperature ($\varepsilon_O \approx 0$), a blocking effect of preadsorbed CO ($\varepsilon_{CO} \approx 1$), and a maximal methanol coverage of $\theta_{MeOH}^{max} = 1$ [42]. For the rate constants of methanol dehydrogenation k_{dehyd} and desorption k_{des}^{MeOH} we write

$$k_{dehyd} = \nu_{dehyd}\exp\left(-\frac{E_{dehyd}}{kT_s}\left(1 - \beta_O\frac{\theta_O}{\theta_O^{max}} - \beta_{CO}\frac{\theta_{CO}}{\theta_{CO}^{max}} - \beta_{MeOH}\frac{\theta_{MeOH}}{\theta_{MeOH}^{max}}\right)\right) \quad (16)$$

and

$$k_{des}^{MeOH} = \nu_{des}^{MeOH}\exp\left(-\frac{E_{des}^{MeOH}}{kT_s}\left(1 - \gamma_O\frac{\theta_O}{\theta_O^{max}} - \gamma_{CO}\frac{\theta_{CO}}{\theta_{CO}^{max}} - \gamma_{MeOH}\frac{\theta_{MeOH}}{\theta_{MeOH}^{max}}\right)\right). \quad (17)$$

Here, the coefficients β_i and γ_i model a possible influence of coadsorbates on the activation energy for desorption and dehydrogenation, respectively.

Under the reaction conditions applied, the coverage of methanol and methoxy is small and, therefore, all dependencies on the methanol coverage can be neglected. Moreover, we can apply a steady state approximation to the methanol/methoxy intermediate, yielding:

$$\theta_{MeOH} = S_{MeOH,eff}^{0}F_{MeOH} \times \frac{\left(1 - \varepsilon_O\frac{\theta_O}{\theta_O^{max}} - \varepsilon_{CO}\frac{\theta_{CO}}{\theta_{CO}^{max}}\right)^{a_{MeOH}}}{k_{des}^{MeOH} + k_{dehyd}\left(1 - \frac{\theta_O}{\theta_O^{max}} - \frac{\theta_{CO}}{\theta_{CO}^{max}}\right)^{a_{dehyd}}}. \quad (18)$$

Employing this model, we have simulated both the steady state and transient experiments for the case of methanol total oxidation. Here, we have used the kinetic parameters from the CO oxidation, as far as they appear in the model. The desorption energy of methanol was estimated as 45–50 kJ mol^{-1} in a previous study [42] and the activation energy for dehydrogenation, which in TPD experiments effectively competes with desorption (see [42] and references therein), is expected to fall within the same range. All other kinetic constant we use as fitting parameters.

A typical set of parameters which provides a good fit to the steady state reaction rates is given in Table 1. A comparison of the simulated steady state reaction rates with the experimental data is displayed in Fig. 10c. In general, we find that the steady state rates are well reproduced by the

model. The behavior under both oxygen-rich and methanol-rich conditions, the temperature dependence, and the magnitude of the turnover frequencies are well described. This is, however, not the case for the transient reaction behavior. Figure 10d shows a comparison of characteristic transients at $x_{\mathrm{MeOH}} = 0.65$. For the simulation, we find a transient trace which is characteristic of the CO-rich regime: CO_2 production maxima are found both upon admission and upon termination of the methanol flux. In the experiment, we observe a pronounced CO_2 peak upon termination, demonstrating that the steady state of the reaction is characterized by a large CO coverage. Surprisingly, there is no rate maximum upon admission of the beam. As already discussed in Section 3.4, we find a slow increase in reaction rate instead.

A systematic analysis shows that no sets of parameters can be found which simultaneously provide a good description of both steady state and transient kinetics. The are two possible explanations for this disagreement. First, the essential steps in kinetic description might be missing or the model might not provide the necessary flexibility, e.g., with respect to coverage dependencies of kinetic parameters. Second, the failure to describe the transient behavior might indicate a breakdown of the mean-field approach.

Specifically, we may consider two contributions to the observed discrepancies: (1) First we may invoke the formation of carbon species. In previous work, we have shown that slow C–O bond scission may occur at defect sites on the particles and the resulting carbon and hydrocarbon species specifically block these sites [43]. As a result, we may expect a slow variation of the dehydrogenation rate upon exposure to methanol. Upon inspection of the transient behavior, however, we find a slow transient increase in the dehydrogenation rate rather than a decrease, which would be expected as a consequence of partial poisoning of the particles by carbon. Moreover, we have observed that carbon accumulation is effectively suppressed at larger oxygen fluxes [42]. Thus, it appears unlikely that the specific transient behavior is due to slow carbon formation alone. (2) As a second non-mean-field effect, we may consider island formation. Upon admission to methanol after extended oxygen exposure, the reaction starts from particles, which are fully covered by an oxygen adlayer, initially. Approaching steady state, partial oxygen and partial CO coverages are established, with islanding behavior depending on the specific reaction conditions. In many cases, surface reactions have been observed to proceed only at specific sites of such adsorbate islands. As an example, Bowker found for methanol oxidation on Cu (110) that the reaction proceeds only at specific border sites of oxygen islands, which are rare on the oxygen-saturated surface [51]. Consequently, the reaction, which is initially slow, shows autocatalytic behavior, similar to what is observed in this work (see Section 3.4). A corresponding refinement of kinetic models is possible on the basis of Monte Carlo simulations, as has been demonstrated, e.g., for the case of CO oxidation on Pt (111) at low temperature [59],

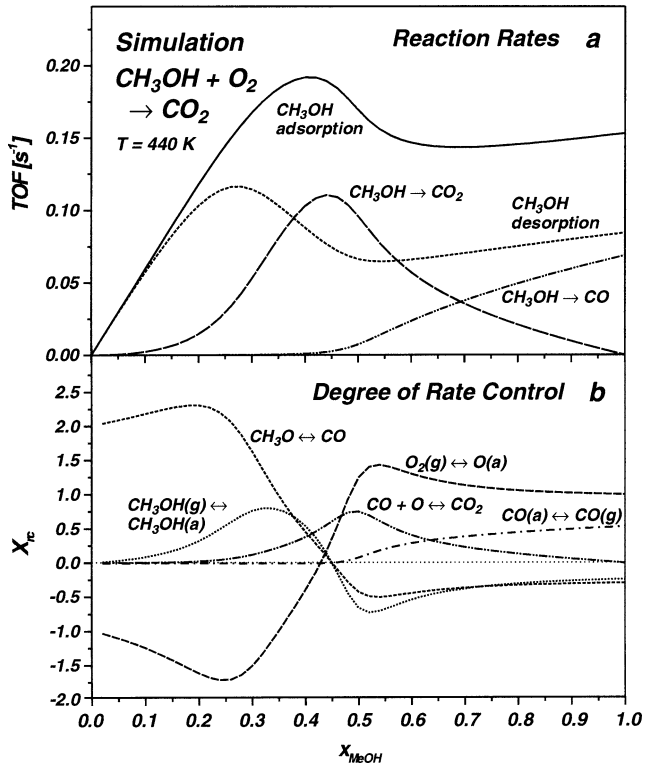

Fig. 11. (a) Calculated rates for different reaction steps during methanol oxidation; (b) calculated degree of rate control of different reaction steps ($T_S = 440$ K).

but additional microscopic information on the reaction structures formed is needed.

As a final point in the discussion we come back to an analysis of the steady state behavior, which is reasonably well described by the kinetic model. In Fig. 11a, we have plotted the predicted rates for different reaction steps as a function of x_{MeOH}. Additionally, we may analyze the kinetics in terms of the rate control of different steps. We follow the definition by Campbell [60,61], who defines the degree of rate control $X_{\mathrm{rc},i}$ of a given step i as

$$X_{\mathrm{rc},i} = \frac{k_i}{r}\left(\frac{\partial r}{\partial k_i}\right)_{K_{\mathrm{eq},i}}. \tag{19}$$

Here, k_i is the rate constant of step i and r is the reaction rate. The derivative is determined at constant equilibrium constant $K_{\mathrm{eq},i}$. The degree of rate control with respect to the total oxidation of methanol, i.e., the rate of CO_2 formation, as determined numerically, is displayed in Fig. 11b.

We find that at high oxygen fluxes ($x_{\mathrm{MeOH}} < 0.3$), a fast chemisorption/desorption equilibrium of methanol is established. The reaction rate is low, as adsorbed oxygen inhibits the dehydrogenation process. (In our model both this is due to the coverage dependence of the reaction barrier and due to a site blocking effect. Taking into account the microscopic insufficiencies of the model, however, these details should not be taken too literally.) The rate controlling step is dehydrogenation, i.e., the breakage of the first C–H bond. As expected, oxygen has a negative degree of rate

control, i.e., a strongly inhibiting effect on the reaction. If we proceed toward larger methanol fluxes ($0.3 < x_{MeOH} < 0.7$), we are approaching the transition between oxygen-rich and CO-rich steady states. As for the CO oxidation, the transition point coincides with the maximum of the CO_2 production rate ($x_{MeOH} < 0.45$). At $x_{MeOH} > 0.45$, CO desorption starts to compete with CO oxidation, leading to the evolution of CO as a second product. The analysis of the degree of rate control shows a complex situation with several processes such as methanol chemisorption, dehydrogenation, CO oxidation, and oxygen adsorption having similar influences on the total rate, which sensitively depend on the reactant fluxes. At high methanol fluxes ($x_{MeOH} > 0.7$), dehydrogenation to CO starts to become the dominating pathway. As expected, the step with the highest degree of rate control is the adsorption of oxygen under these conditions. Finally, it is noteworthy that—in agreement with the isotope exchange experiments described in Section 3.5—the dehydrogenation to CO under conditions of low oxygen fluxes is predicted by the model to proceed with similar turnover frequencies as the oxidation to CO_2 at a higher oxygen ratio.

4. Conclusions

We have utilized molecular beam techniques and in situ TR-IRAS to investigate the kinetics of methanol oxidation on a supported Pd model catalyst. The model catalyst is prepared under UHV conditions on an ordered alumina film grown on NiAl (110). The specific model system under consideration is characterized by particles of average size approximately 5.5 nm, predominantly terminated by Pd (111) facets. The structure and adsorption properties as well as the mechanism of methanol decomposition on this model system have studied previously.

1. In a two-beam experiment we have systematically measured the total oxidation rate of methanol under *steady state* conditions as a function of reactant fluxes and surface temperature. The experiments were combined with in situ static IRAS experiments. A comparison with equivalent experiments for the case of CO oxidation reveals a strongly inhibiting effect of oxygen on the dehydrogenation of methanol.
2. In a two-beam experiment we have performed systematic measurements of the *transient* rate of methanol total oxidation as a function of reactant fluxes and surface temperature. The experiments are combined with TR-IRAS. A comparison with equivalent experiments for the case of CO oxidation shows qualitative differences in the transient behavior, which are associated with a pronounced inhibiting effect of high oxygen precoverages.
3. Three-beam *isotope exchange experiments* combined with detection via TR-IRAS have been performed in order to determine the rate of methanol dehydrogenation to CO under steady state conditions as a function of surface temperature and reactant flux. It is found that under conditions of low oxygen flux, methanol dehydrogenation to CO proceeds with rates similar to those of methanol total oxidation at high oxygen flux.
4. *Microkinetic simulations* of the experiments have been performed on the basis of a mean-field model. The model was constructed in a two-step procedure, including the steady state and transient experimental data for both reaction systems, CO oxidation and methanol oxidation. Validity and limits of the mean-field approach are discussed in connection with deviations found with respect to the oxygen-induced inhibition effect in the transient response.

Acknowledgments

This work has been funded by the Max-Planck-Society and the Deutsche Forschungsgemeinschaft. The authors thank Professor H.-J. Freund for his support of this project.

References

[1] B.C. Bond, Surf. Sci. 156 (1985) 966.
[2] V.P. Zhdanov, B. Kasemo, Surf. Sci. Rep. 39 (2000) 25.
[3] C.R. Henry, Surf. Sci. Rep. 31 (1998) 231.
[4] M. Bäumer, H.-J. Freund, Prog. Surf. Sci. 61 (1999) 127.
[5] C.T. Campbell, A.W. Grant, D.E. Starr, S.C. Parker, V.A. Bondzie, Top. Catal. 14 (2001) 43.
[6] T.P.St. Clair, D.W. Goodman, Top. Catal. 13 (2000) 5.
[7] R.M. Jaeger, H. Kuhlenbeck, H.-J. Freund, M. Wuttig, W. Hoffmann, R. Franchy, H. Ibach, Surf. Sci. 259 (1991) 235.
[8] J. Libuda, F. Winkelmann, M. Bäumer, H.-J. Freund, T. Bertrams, H. Neddermeyer, K. Müller, Surf. Sci. 318 (1994) 61.
[9] M. Frank, M. Bäumer, Phys. Chem. Chem. Phys. 2 (2000) 3723.
[10] I. Meusel, J. Hoffmann, J. Hartmann, M. Heemeier, M. Bäumer, J. Libuda, H.-J. Freund, Catal. Lett. 71 (2001) 5.
[11] S. Shaikhutdinov, M. Heemeier, J. Hoffmann, I. Meusel, B. Richter, M. Bäumer, H. Kuhlenbeck, J. Libuda, H.-J. Freund, R. Oldman, S.D. Jackson, C. Konvicka, M. Schmid, P. Varga, Surf. Sci. 501 (2002) 270.
[12] M.P. D'Evelyn, R.J. Madix, Surf. Sci. Rep. 3 (1984) 413.
[13] M. Asscher, G.A. Somorjai, in: G. Scoles (Ed.), in: Atomic and Molecular Beam Methods, Vol. 2, Oxford University Press, 1988, p. 489.
[14] C.T. Rettner, D.J. Auerbach, J.C. Tully, A.W. Kleyn, J. Phys. Chem. 100 (1996) 13021.
[15] I. Stara, V. Nehasil, V. Matolin, Surf. Sci. 365 (1996) 69.
[16] V. Nehasil, I. Stara, V. Matolin, Surf. Sci. 352 (1996) 305.
[17] L. Piccolo, C.R. Henry, Surf. Sci. 452 (2000) 198.
[18] L. Piccolo, C.R. Henry, Appl. Surf. Sci. 162–163 (2000) 670.
[19] J. Libuda, I. Meusel, J. Hartmann, H.-J. Freund, Rev. Sci. Instrum. 71 (2000) 4395.
[20] J. Libuda, I. Meusel, J. Hoffmann, J. Hartmann, L. Piccolo, C.R. Henry, H.-J. Freund, J. Chem. Phys. 114 (2001) 4669.
[21] I. Meusel, J. Hoffmann, J. Hartmann, J. Libuda, H.-J. Freund, J. Phys. Chem. B 105 (2001) 3567.
[22] J. Hoffmann, I. Meusel, J. Hartmann, J. Libuda, H.-J. Freund, J. Catal. 204 (2001) 378.

[23] M.L. Poutsma, L.F. Elek, P.A. Ibarbia, A.P. Risch, J.A. Rabo, J. Catal. 52 (1978) 157.
[24] J.P. Hindermann, G.J. Hutchings, A. Kiennemann, Catal. Rev. Sci. Eng. 35 (1993) 1.
[25] M.L. Cubeiro, J.L.G. Fierro, J. Catal. 179 (1998) 150.
[26] E.M. Cordi, J.L. Falconer, J. Catal. 162 (1996) 104.
[27] W.J. Shen, M. Okumura, Y. Matsumura, M. Haruta, Appl. Catal. A Gen. 213 (2001) 225.
[28] G.C. Cabilla, A.L. Bonivardi, M.A. Baltanas, Catal. Lett. 55 (1998) 147.
[29] V.L. Kirillov, Y.A. Ryndin, React. Kinet. Catal. Lett. 59 (1996) 351.
[30] A. Gotti, R. Prins, J. Catal. 175 (1998) 302.
[31] R.P. Holroyd, M. Bowker, Surf. Sci. 377–379 (1997) 786.
[32] J.-J. Chen, Z.-C. Jiang, Y. Zhou, B.R. Chakraborty, N. Winograd, Surf. Sci. 328 (1995) 248.
[33] M. Rebholz, V. Matolin, R. Prins, N. Kruse, Surf. Sci. 251 (1991) 1117.
[34] J.L. Davis, M.A. Barteau, Surf. Sci. 235 (1990) 235.
[35] X. Guo, L. Hanley, J.T. Yates Jr., J. Am. Chem. Soc. 111 (1989) 3155.
[36] R.J. Levis, Z.C. Jiang, N. Winograd, J. Am. Chem. Soc. 111 (1989) 4605.
[37] A.K. Bhattacharya, M.A. Chesters, M.E. Pemble, N. Sheppard, Surf. Sci. 206 (1988) L845.
[38] K. Christmann, J.E. Demuth, J. Chem. Phys. 76 (1982) 6318.
[39] K. Christmann, J.E. Demuth, J. Chem. Phys. 76 (1982) 6308.
[40] S.M. Francis, J. Corneille, D.W. Goodman, M. Bowker, Surf. Sci. 364 (1996) 30.
[41] M. Mavrikakis, M.A. Barteau, J. Mol. Catal. A 131 (1998) 135.
[42] S. Schauermann, J. Hoffmann, V. Johánek, J. Hartmann, J. Libuda, Phys. Chem. Chem. Phys. 4 (2002) 3909.
[43] S. Schauermann, J. Hoffmann, V. Johánek, J. Hartmann, J. Libuda, H.-J. Freund, Angew. Chem. Int. Ed. 41 (2002) 2532.
[44] D.A. King, M.G. Wells, Surf. Sci. 29 (1972) 454.
[45] D.A. King, M.G. Wells, Proc. R. Soc. London Ser. A 339 (1974) 245.
[46] R.M. Jaeger, J. Libuda, M. Bäumer, K. Homann, H. Kulenbeck, H.-J. Freund, J. Electron Spectrosc. Relat. Phenom. 64/65 (1993) 217.
[47] K. Wolter, O. Seiferth, H. Kuhlenbeck, M. Bäumer, H.-J. Freund, Surf. Sci. 399 (1998) 190.
[48] J. Libuda, H.-J. Freund, J. Phys. Chem. B 106 (2002) 4901.
[49] F.M. Hoffmann, Surf. Sci. Rep. 3 (1983) 107.
[50] K.T. Queeney, C.M. Friend, J. Chem. Phys. 109 (1998) 6067.
[51] M. Bowker, Top. Catal. 3 (1996) 461.
[52] L. Piccolo, C. Becker, C.R. Henry, Appl. Surf. Sci. 164 (2000) 156.
[53] C. Becker, C.R. Henry, Surf. Sci. 352–354 (1996) 457.
[54] C. Becker, C.R. Henry, Catal. Lett. 43 (1997) 55.
[55] T. Engel, J. Chem. Phys. 69 (1978) 373.
[56] S. Shaikhutdinov, M. Heemeier, M. Bäumer, T. Lear, D. Lennon, R.J. Oldman, S.D. Jackson, H.-J. Freund, J. Catal. 200 (2001) 330.
[57] H. Conrad, G. Ertl, J. Küppers, Surf. Sci. 76 (1978) 323.
[58] M. Eriksson, L.-G. Ekedahl, Surf. Sci. 412/413 (1998) 430.
[59] S. Völkening, J. Wintterlin, J. Chem. Phys. 114 (2001) 6382.
[60] C.T. Campbell, Top. Catal. 1 (1994) 353.
[61] C.T. Campbell, J. Catal. 204 (2001) 520.